Journal of Volcanology and Geothermal Research 319 (2016) 1–11

Contents lists available at ScienceDirect

Journal of Volcanology and Geothermal Research

journal homepage: www.elsevier.com/locate/jvolgeores

The strength of heterogeneous volcanic rocks: A 2D approximation

Michael J. Heap [a,*], Fabian B. Wadsworth [b], Tao Xu [c], Chong-feng Chen [c], Chun'an Tang [d]

[a] Géophysique Expérimentale, Institut de Physique de Globe de Strasbourg (UMR 7516 CNRS, Université de Strasbourg/EOST), 5 rue René Descartes, 67084 Strasbourg cedex, France
[b] Earth & Environmental Sciences, Ludwig-Maximilians-Universität, Theresienstr. 41/III, 80333 München, Germany
[c] Center for Rock Instability and Seismicity Research, Northeastern University, Shenyang 110819, China
[d] School of Civil and Hydraulic Engineering, Dalian University of Technology, Dalian 116024, China

ARTICLE INFO

Article history:
Received 22 October 2015
Received in revised form 7 March 2016
Accepted 16 March 2016
Available online 18 March 2016

Keywords:
Pore
Crystal
Uniaxial compressive strength
Numerical modelling
Effective medium approach

ABSTRACT

Volcanic rocks typically contain heterogeneities in the form of crystals and pores. We investigate here the influence of such heterogeneity on the strength of volcanic rocks using an elastic damage mechanics model in which we numerically deform two-dimensional samples comprising low-strength elements representing crystals and zero-strength elements representing pores. These circular elements are stochastically generated so that there is no overlap in a medium representing the groundmass. Our modelling indicates that increasing the fraction of pores and/or crystals reduces the strength of volcanic rocks, and that increasing the pore fraction results in larger strength reductions than increasing the crystal fraction. The model also highlights an important weakening role for pore diameter, but finds that crystal diameter has a less significant influence for strength. To account for heterogeneity (pores and crystals), we propose an effective medium approach where we define an effective pore fraction $\phi_p' = V_p/(V_p + V_g)$ where V_p and V_g are the pore and groundmass fractions, respectively. Highly heterogeneous samples (containing high pore and/or crystal fractions) will therefore have high values of ϕ_p', and vice-versa. When we express our numerical samples (more than 200 simulations spanning a wide range of crystal and pore fractions) in terms of ϕ_p', we find that their strengths can be described by a single curve for a given pore diameter. To provide a predictive tool for the strength of heterogeneous volcanic rocks, we propose a modified version of 2D solution for the Sammis and Ashby (1986) pore-emanating crack model, a micromechanical model designed to estimate strength using microstructural attributes such as porosity, pore radius, and fracture toughness. The model, reformulated to include ϕ_p' (and therefore crystal fraction), captures the strength curves for our numerical simulations over a sample heterogeneity range relevant to volcanic systems. We find that published experimental data (for which the porosity and crystal fraction is known) correlate well with our modelled curves, adding validity to our approach. We present herein a 2D analytical tool to estimate the strength of volcanic rock that can be used when the porosity, crystal fraction, and maximum pore diameter are known.

1. Introduction

A volcanic edifice is constructed from the products of successive effusive and/or explosive events and endogenous intrusions (Borgia and Linneman, 1990; Kaneko, 2002; Biggs et al., 2010; Odbert et al., 2015). The structural stability of this structure — its predisposition for devastating collapse — relies, in part, on the strength of these materials (Voight and Elsworth, 1997; Voight, 2000). The volcanic rocks forming the edifice are typically heterogeneous, a consequence of their complex genesis, and often contain crystals and pores of varying size, shape, and abundance. The result of this vast heterogeneity is that the compressive strength of volcanic materials can vary from a couple of MPa (e.g., Heap et al., 2012) to many hundred MPa (e.g., Vasseur et al., 2013).

The abundance (e.g., Kueppers et al., 2005; Wright et al., 2009; Farquharson et al., 2015; Lavallée et al., 2016) and diameter (e.g., Wright et al., 2009; Shea et al., 2010; Heap et al., 2014a) of pores within volcanic rocks varies tremendously. These pores are the frozen relicts of gas exsolution in ascending magma (e.g., Sparks, 1978; Toramaru, 1989; Mangan and Cashman, 1993; Navon and Lyakhovsky, 1998; Gonnermann and Manga, 2013) or those remaining after partial welding (Wadsworth et al., 2014). The porosity of an extruded (and cooled) volcanic rock is a function of numerous intertwined factors during its genesis, including the initial dissolved volatile content in the magma, the rate of ascent (dependent on volatile content, crystal content, and melt viscosity, amongst others; see Gonnermann and Manga, 2013 and references therein), and the ability of the magma to outgas either up through the conduit or laterally into the country rock (Jaupart, 1998). The diameter of the preserved pores, and their diameter size distribution, also depends on numerous interconnected factors: the melt viscosity, the magma volatile content and type, and decompression

* Corresponding author.
E-mail address: heap@unistra.fr (M.J. Heap).

http://dx.doi.org/10.1016/j.jvolgeores.2016.03.013
0377-0273/© 2016 Published by Elsevier B.V.

rate, amongst others (e.g., Shea et al., 2010; Gondé et al., 2011; Gonnermann and Manga, 2013 and references therein). The result of this extremely complex genesis is that the porosity of volcanic rocks can range from almost 0 to almost 1 (e.g., Kueppers et al., 2005; Wright et al., 2009; Farquharson et al., 2015; Lavallée et al., 2016), and pore diameter can span multiple orders of magnitude (typically from a few tens of microns to a few mm; Wright et al., 2009; Shea et al., 2010; Heap et al., 2014a). We note that "mega vesicles" can be several tens of cm (Self et al., 1997 and references therein).

The abundance and size of crystals within volcanic rocks also varies tremendously (Marsh, 1988), both of which depend on the kinetics of crystal nucleation and growth in the magma from which they form. Crystals will nucleate in magma when the melt phase is sufficiently undercooled or supersaturated; the rate of nucleation is controlled by the degree of undercooling and supersaturation and directly affects the resultant crystal number density and growth rate (e.g., Spohn et al., 1988) and, therefore, the final size distribution (Marsh, 1988; Cashman and Marsh, 1988; Gonnermann and Manga, 2013). Such undercooling is often a consequence of exsolution of magmatic volatile phases (Applegarth et al., 2012; Hammer, 2004). Additionally, nucleation and growth of anhydrous crystal phases act as a positive feedback by further enriching the melt in volatiles or inhibiting cooling (Blundy et al., 2006). Since the volatile, bubble, and crystal content of the melt all impact the suspension viscosity (Hess and Dingwell, 1996; Mader et al., 2013), devolatilisation and crystallisation are complex and coupled processes that feedback to one another during shallow magma ascent. The consequence of this complex and varied genesis is that the crystal content of volcanic rocks can also range from almost 0 to almost 1 (e.g., Marsh, 1981; Brophy, 1991; Blundy et al., 2006). Additionally, crystal sizes typically vary from phenocrysts (greater than 0.5 mm in length) to microlites (less than 0.1 mm) (e.g., Cashman and Marsh, 1988). We note that "megacrysts" can be several cm (e.g., Gutmann, 1977).

The strength of volcanic rocks is known scale with porosity (e.g., Al-Harthi et al., 1999; Heap et al. 2014a,b; Schaeffer et al., 2015) and pore diameter (e.g., Vasseur et al., 2013; Heap et al., 2014b). However, while crystal content has been shown to be an important factor controlling the rheology and onset of brittle behaviour in magmas (Caricchi et al., 2007; Lavallée et al., 2007, 2008; Cordonnier et al., 2009, 2012; Kendrick et al., 2013), the influence of crystal content and size on the strength of volcanic rocks remains poorly constrained. Isolating the influence of a particular parameter on the strength of volcanic rocks, in order to understand their various contributions, is challenging due to their highly variable nature. For example, a suite of samples with different porosity may also contain different pore and crystal size distributions and/or different crystal contents. With the aim of understanding the influence of such heterogeneity (pores and crystals) on the strength of volcanic rocks, we have used the Rock Failure and Process Analysis code ($RFPA_{2D}$) model (e.g., Tang, 1997), a numerical model based on elastic damage mechanics. We use the model to deform two-dimensional numerical samples that consist of heterogeneities — low strength elements representing crystals and zero-strength elements representing pores — that are stochastically generated in a medium representing the groundmass. The $RFPA_{2D}$ model has been previously used to investigate the influence of porosity and pore diameter (Heap et al., 2014b) and pore overpressure (Heap et al., 2015a) on the strength of volcanic materials.

2. Description of the model: rock failure and process analysis code ($RFPA_{2D}$)

The $RFPA_{2D}$ model (e.g., Tang, 1997) assumes that the volcanic rock modelled herein reacts in an elastic and brittle manner to an external stress. Indeed, we anticipate that volcanic rocks of the edifice reside at temperatures sufficiently low to ensure the groundmass is quenched to a glass or is microcrystalline, and that any temperature fluctuations will rarely exceed the glass transition. The numerical samples are deformed uniaxially in our simulations (see below section) and our output should only therefore be applied to deformation within the upper edifice (>1 km) where the rocks dilate in response to a differential stress. Compactant micromechanisms, such as cataclastic pore collapse, are likely to dictate the deformation of porous rock deeper in the edifice (Heap et al., 2015b).

2.1. Description of the numerical samples

This paper aims to tackle the impact of heterogeneity on strength by complementing the simulations presented in Heap et al. (2014b), which address the influence of porosity and pore diameter on the strength of crystal-free rocks, with new simulations designed to address the influence of crystal size and crystal content on the strength of volcanic rocks.

All of the numerical simulations presented in this study uniaxially deform a two-dimensional rectangular sample, 40 mm in length and 20 mm in width (consisting of 80,000 square elements with sides of 0.1 mm). The generated samples comprise a groundmass that can be populated with pores and/or crystals. The groundmass of each sample was assigned the same macroscopic physical and mechanical properties (Table 1). To reflect microscale material heterogeneity (small length-scale variations in microlite number density and size, or glass strength), each 0.1 mm square element was assigned a value of strength (compressive σ_{cr} and tensile σ_{tr}) and Young's modulus E_0 using a Weibull probability density function (Weibull, 1951; Wong et al., 2006):

$$x(u) = \frac{m}{u_0}\left(\frac{u}{u_0}\right)^{m-1}\exp\left[-\left(\frac{u}{u_0}\right)^{m}\right], \tag{1}$$

where $x(u)$ is either $\sigma_{cr}(u)$, $\sigma_{tr}(u)$, or $E_0(u)$ and u and u_0 are the scale parameter of an individual element and the scale parameter of the average element, respectively (which both depend on the parameter in question). We chose to let the groundmass homogeneity factor m, the Weibull shape parameter, to be 3 in all of our numerical simulations (more discussion on m is provided in Xu et al., 2012 and Heap et al., 2015a). The modelled output showed that the strength of a porosity-free numerical sample (553 MPa, see Heap et al. 2014b) is close to that of an experimentally deformed borosilicate glass (~600 MPa, see Vasseur et al., 2013), serving to validate our choice of macroscopic physical and mechanical properties (Table 1) and shape parameter m.

Porosity was introduced in the form of circular pores, which were placed in the groundmass at random and without overlap. The two-phase (groundmass and pores) simulations of Heap et al. (2014b) used porosities of 0.02, 0.05, 0.1, 0.2, 0.25, 0.3, 0.35, and 0.4. For each value of porosity, samples that contained pore diameters of 0.1, 0.3, 0.5, and 1 mm were prepared (a total of 36 different combinations). The simulations unique to this study were either two-phase (groundmass and crystals) or three-phase (groundmass, pores, and crystals). The crystals, circular in shape, were introduced first. We chose to create samples containing crystal fractions of 0.02, 0.05, 0.1, 0.15, 0.2, 0.25, 0.3, 0.35, or 0.4, which were placed in the numerical samples at random and without overlap. The macroscopic physical and mechanical properties

Table 1
The physical and mechanical properties of the groundmass used in the Rock Failure and Process Analysis code ($RFPA_{2D}$) numerical modelling. The same input values as in Heap et al. (2014b).

Homogeneity index	3
Mean uniaxial compressive strength [MPa]	2300
Mean Young's modulus [GPa]	100
Poisson's ratio	0.25
Ratio of compressive to tensile strength	10
Frictional angle [degrees]	30

Table 2
The physical and mechanical properties of the crystals used in the rock failure and process analysis code ($RFPA_{2D}$) numerical modelling.

Homogeneity index	1
Uniaxial compressive strength [MPa]	1250
Young's modulus [GPa]	70
Poisson's ratio	0.25
Ratio of compressive to tensile strength	10
Frictional angle [degrees]	30

of the crystals (Table 2) were chosen so that the crystals were weaker than the groundmass. We lowered the strength, the Young's modulus, and reduced homogeneity factor *m* to make the crystals more heterogeneous than the groundmass. Crystals in volcanic rocks often contain microcracks and defects (plagioclase crystals, for example, can be twinned and are often fractured). Indeed, previous experimental studies on the brittle deformation of volcanic materials have shown pervasive microcracking in the crystal phase (e.g., Lavallée et al., 2007). The $RFPA_{2D}$ model determined that a sample composed of a crystal fraction of 1 (i.e., porosity-free) had a uniaxial compressive strength of 125 MPa, compared to 553 MPa for a sample containing a groundmass fraction of 1 (i.e., crystal-free; Heap et al. 2014b). For each value of crystal content, we generated samples that contained crystal diameters of 0.3, 0.5, 1.0, 1.5, or 2.0 mm. For the three-phase rocks, there was a final step: the addition of porosity as circular pores. The circular pores were placed so that there was no overlap with the crystal phase or each other. We used porosity fractions of 0.05, 0.1, and 0.25 and pore diameters of either 0.5 or 1 mm. We note that the model was unable to generate samples with high porosities and high crystal fractions. In total, we performed over 200 simulations (with almost 150 unique to this study).

Examples of the two-phase (groundmass and pores, and groundmass and crystals) and three-phase (groundmass, pores, and crystals) numerical samples are provided as Fig. 1.

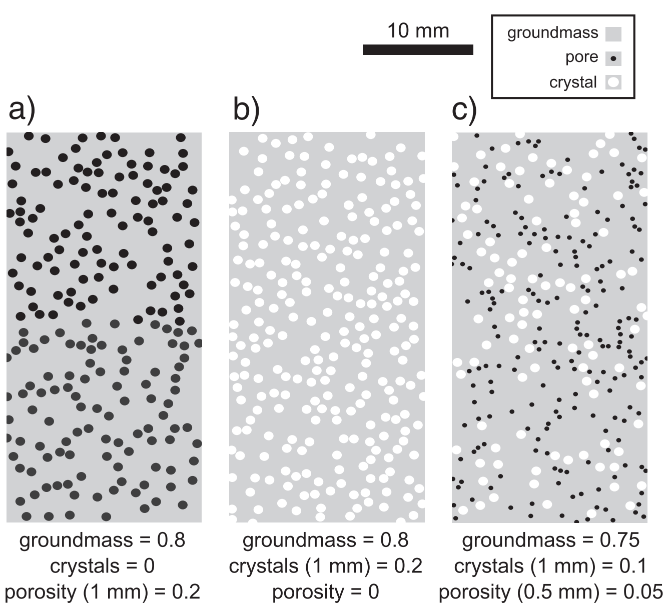

Fig. 1. Examples of the numerically generated samples. Samples are 40 mm long and 20 mm in diameter. (a) Two-phase sample containing a porosity of 0.2 (diameter 1 mm). (b) Two-phase sample containing a crystal fraction of 0.2 (diameter 1 mm). (c) Three-phase sample containing a porosity of 0.05 (diameter 0.5 mm) and a crystal fraction of 0.1 (diameter 1 mm).

2.2. Deforming the numerical samples

The numerical samples were deformed uniaxially ($\sigma_1 > \sigma_2$ and $\sigma_2 = \sigma_3 = 0$) in 0.002 mm increments (corresponding to axial strain increments of 0.005%). Following each uniaxial loading increment, the stress acting on each 0.1 mm element was calculated. If no elements were damaged in a particular loading increment, the numerical sample was subjected to the next 0.002 mm displacement increment. However, if the stress acting on a particular element met one of the two strength criteria (the maximum tensile strain criterion and the Mohr–Coulomb criterion), the element was considered damaged and its Young's modulus modified according to an elastic damage constitutive law (see Lemaitre and Chaboche, 1990; Xu et al., 2012; Heap et al. 2014b, 2015a). The tensile strength criterion was more likely to be met since the tensile strength has been set as a tenth of the compressive strength (Tables 1 and 2; Jaeger et al., 2007). If any elements were damaged, the distribution of stress within the sample was recalculated. The stress was continually recalculated until no further elements were damaged, at which point the numerical sample was subjected to the next 0.002 mm displacement increment. As a result, there is no deformation rate *sensu stricto*: the numerical samples are deformed so that the rate of deformation does not exceed the evolution of the microstructure. By implication, the model may not accurately capture the mechanical behaviour of rapidly deforming rocks adjacent to the conduit. This procedure continued until macroscopic sample failure (i.e., the formation of a throughgoing fracture). In this study we adopt the convention that compressive stresses and strains are positive. In the following sections we present in turn the influence of (1) heterogeneity content and, (2) heterogeneity diameter on the strength of two- and three-phase volcanic rocks.

3. The influence of heterogeneity (pores and crystals) content on strength

The influence of porosity and crystal fraction on uniaxial compressive strength is summarised in Fig. 2. Fig. 2a shows the influence of pores in a two-phase volcanic rock (i.e., crystal-free rock; simulation output from Heap et al. 2014b). We see that, for a pore diameter of 0.5 mm, the compressive strength is reduced from 358 MPa at a porosity of 0.02 to 47 MPa at a porosity of 0.4 (Fig. 2a). Porosity therefore exerts a significant control on the uniaxial compressive strength of volcanic rocks (as reported in the experimental studies of Al-Harthi et al., 1999; Heap et al., 2014a; Schaeffer et al., 2015). Fig. 2b illustrates the influence of crystals on the strength of two-phase volcanic rock (i.e., porosity-free rock) for a sample with a crystal diameter of 1 mm. Strength is reduced from 458 to 337 MPa upon increasing the crystal fraction from 0.02 to 0.4 (Fig. 2b). Taken together, Fig. 2a and b highlights that the strength of volcanic rocks is more influenced by the pore fraction than crystal fraction. Indeed, increasing the pore fraction from 0.02 to 0.4 reduces strength by a factor of 7.6, while increasing the crystal fraction from 0.02 to 0.4 reduces strength by only a factor of 1.4. Fig. 2c shows simulation output for a three-phase system of groundmass, pores, and crystals. In detail, Fig. 2c presents the influence of crystal fraction (crystal diameter = 1 mm) on uniaxial compressive strength for different values of porosity (0.05, 0.1, and 0.25; pore diameter = 0.5 mm). For each of the tested porosities (0.05, 0.1, and 0.25), increasing the crystal fraction decreases the strength of three-phase volcanic rocks. For example, at a constant porosity of 0.1, increasing the crystal fraction from 0.02 to 0.4 decreases the strength from 177 to 128 MPa. Likewise, increasing the porosity for a given crystal fraction also results in a strength reduction (Fig. 2c). For example, at a crystal fraction of 0.2, increasing the porosity from 0.05 to 0.25 decreases the strength from 191 to 70 MPa.

We will first discuss why increasing the porosity lowers the strength of two-phase (i.e., crystal-free) volcanic rocks (Fig. 2a; simulation output from Heap et al. 2014b). The presence of pores locally amplifies the stress within the groundmass (Jaeger et al., 2007; Sammis and

Ashby, 1986). As the macroscopic stress is increased on the sample, these local, amplified stress fields facilitate the nucleation of pore-emanating microcracks (as shown in the deformation snapshot of Fig. 3b). In other words, the highly stressed elements at the pore wall are the first elements to fail in the model. Once a microcrack is initiated, it grows as the sample is further deformed due to the amplified stresses at the tip of the microcrack (Fig. 3c and d). Eventually these pore-emanating microcracks can interact, coalesce, and conspire to macroscopically fail the sample (Fig. 3e). We often find that microcracks nucleate within clusters or chains of pores (see Fig. 3c), a result of the overlap of the stress amplification fields of neighbouring pores. Stress field interaction further magnifies the stress and promotes microcrack initiation and growth at lower applied stresses. As porosity increases, not only do the samples contain more void space, meaning that macroscopic failure requires the failure of fewer elements (microcracks can easily jump from pore to pore), but the likelihood of pore clustering and stress field overlap increases (as discussed in Heap et al. 2014b). Although increasing the porosity will reduce the average element strength, we highlight that the first elements to break are the weakest elements within the groundmass (as defined by the parameters given in Table 1). An increase in the porosity will not alter the proportion of very weak groundmass elements within the sample.

There are a couple of reasons why an increase in crystal fraction could result in the observed decrease in strength in two-phase (i.e., porosity-free) volcanic rocks (Fig. 2b). First, as the crystal fraction increases, the proportion of elements with a very low strength (as defined by the parameters given in Table 2), which fail at low stresses and act as failure nuclei from which fractures can grow (Fig. 4), will increase. Second, there is an increased likelihood that crystals will form clusters or chains as the crystal fraction increases. As mentioned above, we notice that deformation is often first accommodated by the very weak elements within crystals (Fig. 4b; present due to a combination of their low strength and low heterogeneity index *m*; Table 2). Damaged elements increase the stress on neighbouring elements, quickly facilitating the formation of intracrystalline microcracks and/or highly damaged crystals (Fig. 4c). If there is a cluster or chain of crystals, intracrystalline microcracks can coalesce and form the basis of a throughgoing fracture (as shown in Fig. 4c-e).

For three-phase volcanic rocks, we find that the addition of either pores or crystals results in additional weakening (Fig. 2c). As explained above, the addition of crystals will increase the proportion of very low strength elements and the likelihood of crystal clusters and chains. Likewise, the addition of pores will provide a shorter route for macroscopic failure and will facilitate microcrack nucleation by creating lobes of stress amplification. However, the interaction of these heterogeneities leads to additional weakening. First, when the zone of stress concentration surrounding a pore ensnares a crystal, the weak elements within the crystal (elements within the crystals can be much weaker than those in the groundmass, see Tables 1 and 2) can become damaged during the early stages of deformation even when the applied stress is very low. Crystals sandwiched between two pores are often preferentially damaged and promote pore coalescence by microcracking and, ultimately, the formation of a throughgoing fracture (the snapshots of Fig. 5 show how crystal clusters and chains trapped between pores can promote the formation of a macroscopic fracture). An increase in pore or crystal fraction will therefore increase the chance that a crystal will exist within the perturbed stress field of a pore. Second, since the crystals are generated before the pores, a high crystal fraction can force pore clustering and encourage pore stress field interactions, even at relatively low values of porosity.

4. The influence of heterogeneity (pores and crystals) diameter on strength

The influence of pore and crystal diameter on uniaxial compressive strength of two-phase volcanic rocks is summarised in Fig. 6. Fig. 6a shows the influence of pore diameter on two-phase volcanic rock

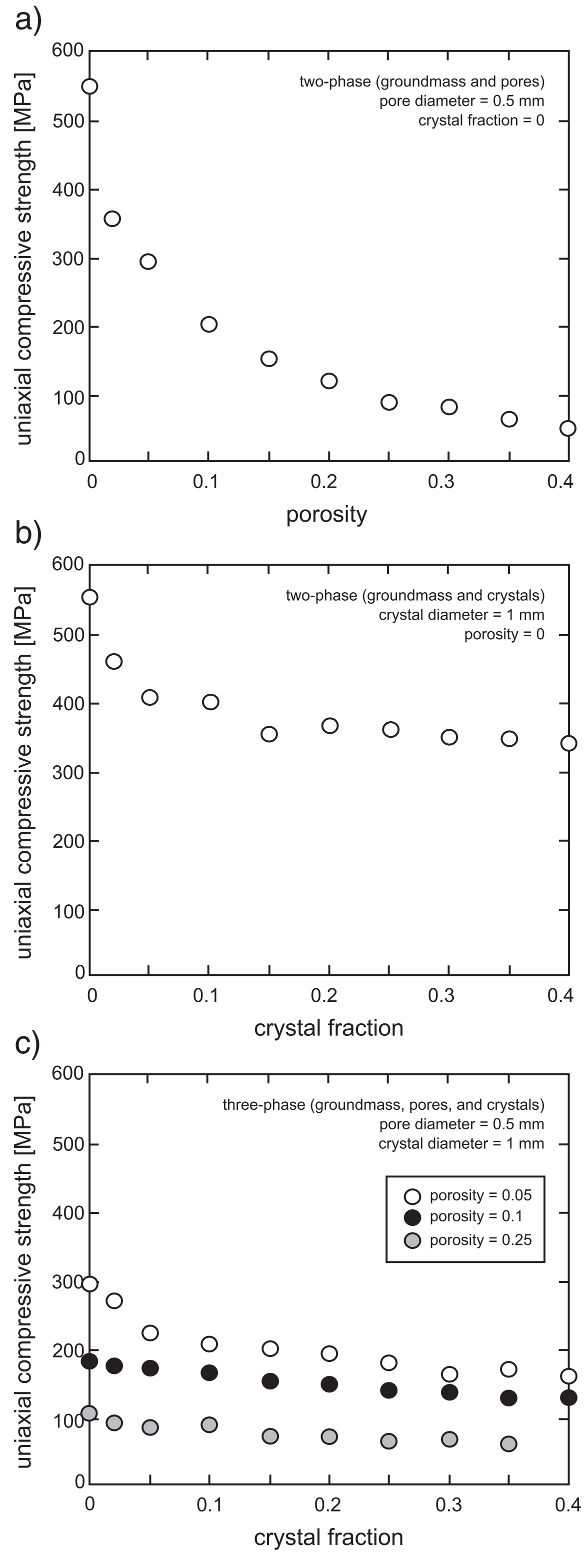

Fig. 2. The influence of heterogeneity content (pores and crystals) on the strength of volcanic rocks. (a) A plot of uniaxial compressive strength as a function of porosity for two-phase (groundmass and pores) simulations (simulation output from Heap et al., 2014b). (b) A plot of uniaxial compressive strength as a function of crystal fraction for two-phase (groundmass and crystals) simulations. (c) A plot of uniaxial compressive strength as a function of crystal fraction for three-phase (groundmass, pores, and crystals) simulations. White circles — simulations containing a porosity of 0.05; black circles — 0.1 porosity; and grey circles — 0.25 porosity.

two-phase (groundmass and pores); porosity = 0.02; pore diameter = 1 mm

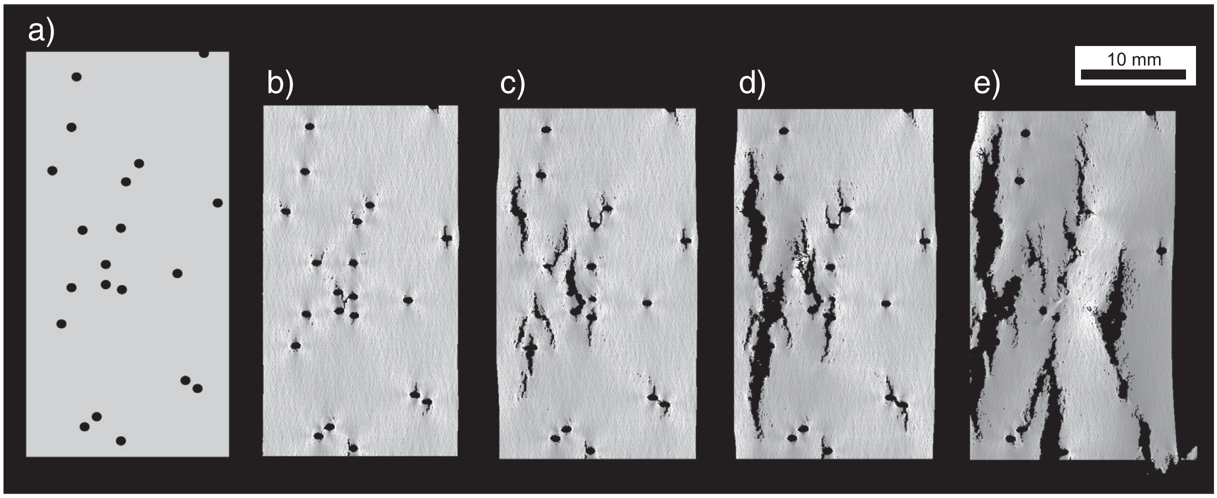

Fig. 3. Deformation snapshots showing the damage evolution of a two-phase (groundmass and pores) numerical sample. (a) The pre-deformation sample (groundmass in grey and pores in black). (b–e) Deformation snapshots at increasing axial strain.

(i.e., crystal-free rock). For a constant value of porosity (0.02, 0.2, and 0.4 are shown here), an increase in pore diameter reduces the strength (Fig. 6a). For example, for a porosity of 0.2, strength is reduced from 334 to 72 MPa as pore diameter is increased from 0.1 to 1 mm. Fig. 6b presents the influence of crystal diameter on two-phase volcanic rock. Fig. 6b shows that the decrease in strength with increasing crystal fraction (from 0.02 to 0.4) is essentially identical for samples containing either 1 or 2 mm diameter crystals (we note that our modelled output demonstrates that crystals of diameter 0.3 and 0.5 mm also do not influence strength at a given crystal fraction). The model output presented in Fig. 6a and b highlights that the strength of volcanic rocks is significantly influenced by pore diameter, but is largely unaffected by crystal diameter.

The influence of crystal and pore diameter on the strength of three-phase volcanic rocks is presented as Fig. 7. Fig. 7a shows the influence of crystal diameter on the strength of three-phase volcanic rocks (for a constant pore diameter and porosity of 0.5 mm and 0.05, respectively) for different crystal fractions (0.02, 0.2, and 0.4). We find that, as for the two-phase rocks of Fig. 6b, increasing the crystal diameter does not affect the strength. Further, this is true for all of the crystal fractions tested (for clarity, only 0.02, 0.2, and 0.4 are shown in Fig. 7a) and when the porosity is increased (Fig. 7b). Fig. 7b shows the influence of crystal diameter on the strength of three-phase volcanic rocks (for a constant pore diameter and crystal fraction of 0.5 mm and 0.2, respectively) for different porosities (0.05 and 0.25). The model output shows that the influence of crystal diameter is negligible at a porosity of 0.05 and 0.25 (Fig. 7b). Fig. 7c shows the influence of pore diameter on the strength of three-phase volcanic rocks (for a constant porosity of 0.25 and pore diameter of 0.5 mm) by comparing model output for two-phase volcanic rock (crystal fraction = 0; simulation output from Heap et al. 2014b) with that for three-phase rock (crystal fraction = 0.25 and crystal diameter = 1 mm). The model output shows that increasing pore diameter reduces the strength of three-phase volcanic rocks, and in a similar way to that found for two-phase rocks. The offset between the two curves simply reflects the weakening influence of a crystal fraction of 0.25.

two-phase (groundmass and crystals); crystal fraction = 0.2; crystal diameter = 1 mm

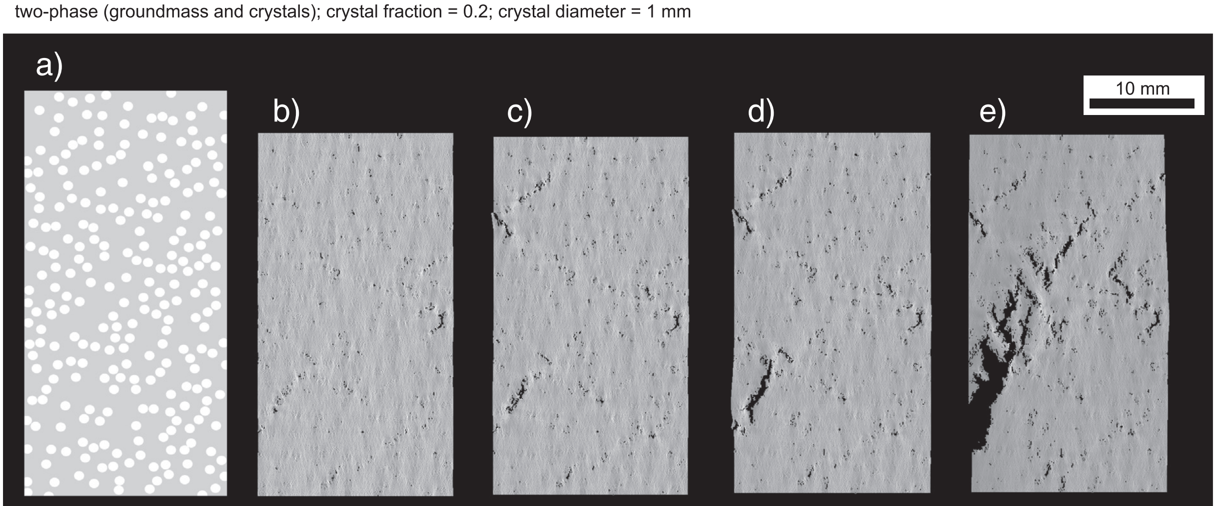

Fig. 4. Deformation snapshots showing the damage evolution of a two-phase (groundmass and crystals) numerical sample. (a) The pre-deformation sample (groundmass in grey and crystals in white). (b–e) Deformation snapshots at increasing axial strain.

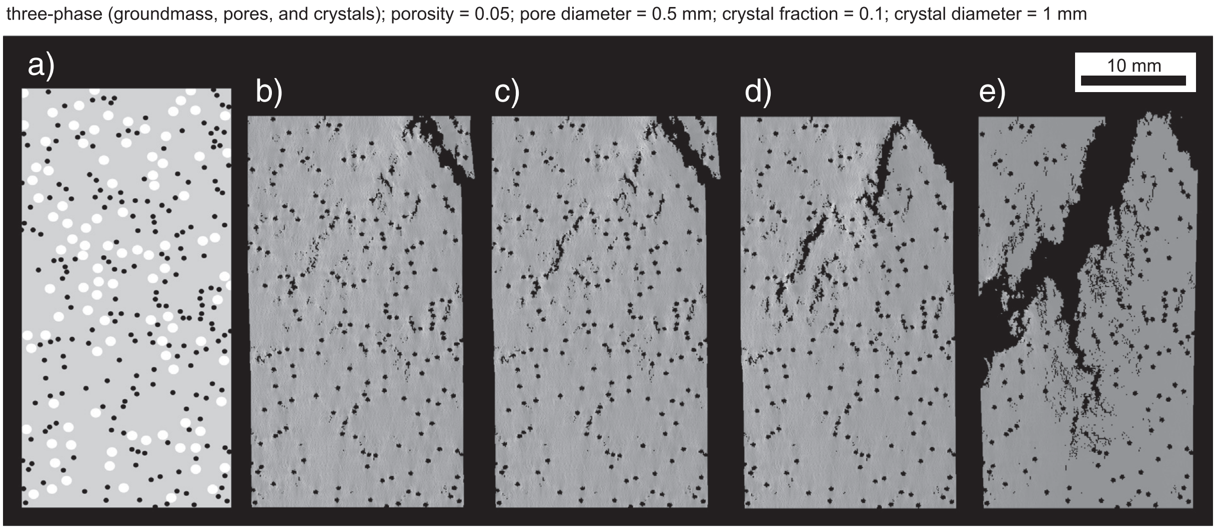

Fig. 5. Deformation snapshots showing the damage evolution of a three-phase (groundmass, pores, and crystals) numerical sample. (a) The pre-deformation sample (groundmass in grey, pores in black, and crystals in white). (b–e) Deformation snapshots at increasing axial strain.

We will first discuss why increasing the pore diameter lowers the strength of two-phase (i.e., crystal-free; Fig. 6a) and three-phase (Fig. 7c) volcanic rocks. Pores with a larger diameter magnify the stress of a larger area (perturbations in the stress field can be considered negligible at distances greater than ten times the diameter; Jaeger et al., 2007). This implies that, at a constant porosity, larger pores create more stress field overlap than smaller pores, or that the fewer, larger stress concentration lobes of the larger pores increase the likelihood that weaker elements are found within the area of stress concentration (as explained in Heap et al. 2014b). In addition, the small stress concentration lobes of smaller pores may not be able to reach the area in the centre of the crystals in the three-phase rocks, especially when the pore diameter is smaller than the crystal diameter; the crystal centres will not be shielded from larger diameter pores that command larger stress concentration lobes.

However, perhaps there is little reason why, for a given crystal fraction, a higher crystal diameter would influence strength of two- (Fig. 6b) or three-phase volcanic rocks (Fig. 7a and b). First, the proportion of very weak elements will be virtually identical. Second, whereas larger pores perturb the stress of a broader area than smaller pores (Sammis and Ashby, 1986; Jaeger et al., 2007; Heap et al. 2014b, 2015a), encouraging elements to fail and microcracks to form through stress field interactions (Heap et al. 2014b), larger crystals do not impart such an effect because the strength differential between crystals and groundmass is not as large as that between pores and groundmass. Third, we have seen that localisation typically initiates from clusters or chains of crystals adjacent to pores. However, for a larger crystal diameter, there is no reason why the crystals would be closer to the pores or, more pertinently, why a greater crystal area would exist within a stress field of a pore. This is especially true when one considers that the pore diameter (0.5 mm), and therefore the size of the perturbed stress field surrounding each pore, is identical between the presented simulations.

5. An effective medium model for the strength of heterogeneous volcanic rocks

We have shown that heterogeneities — namely pores (Fig. 2a) and crystals (Fig. 2b) — can reduce the strength of two-phase volcanic rocks. When both heterogeneities are present, they both conspire to weaken the material (Fig. 2c). It is clear that, since most volcanic rocks contain both pores and crystals, an approach is needed to represent the combination of pores and crystals within a rock as a single variable: "heterogeneity". To achieve this, we propose an effective medium approach.

Up until now, we have defined the crystal ϕ_c and the pore ϕ_p fractions as bulk properties such that $\phi_c = V_c/V_T = V_c/(V_c + V_p + V_g)$ and $\phi_p = V_p/V_T = V_p/(V_c + V_p + V_g)$ where the volumes V_c, V_p, V_g and V_T are the crystal, pore, groundmass without the crystals or pores, and total volumes, respectively. If we instead redefine the fractions to find the effective pore fraction, $\phi_p' = V_p/(V_p + V_g)$, then we can assess both the effect of crystal- and pore-loading on the sample. This is a similar method to that proposed for the assessment of the viscosity of multi-phase systems (Truby et al., 2015). Defining the porous groundmass as an effective continuous medium with a crystal cargo might imply that the pores are much smaller than the crystals, however, Truby et al. (2015) find that this method works for magmas where crystals and pores are similar sizes, as in our simulations. This approach results in Fig. 8a, where we can plot the modelled strength as a function of the effective pore fraction ϕ_p' which accounts for the total heterogeneity of the system as, for example, the addition of crystals to a sample with a fixed porosity serves to increase ϕ_p' by crowding the porosity in the groundmass. To a good approximation, we find that the model output can be described by a single curve for a given pore diameter (we provide model output for a samples containing either 0.5 or 2 mm diameter pores) in the groundmass (Fig. 8a). Because the effective pore fraction is a void fraction of the groundmass, not including the crystal fraction, this has the implication that the strength of the numerical samples is dominated by the effect of the pores, the conclusion drawn from the model output of Fig. 2. Additionally, if we consider these samples as variably heterogeneous materials, then it is certainly the pore fraction, with zero strength, that imparts the larger mean heterogeneity, compared with the crystals, which are a lot closer to the strength of the groundmass. Therefore, we are satisfied that our scaling is consistent with intuitive considerations of the nature of the samples. In Fig. 8a we show these scaling considerations for a given pore diameter produce inter-sample consistency across a wide range of effective pore fractions.

The pore-emanating crack model derived by Sammis and Ashby (1986) can be used to help better understand the micromechanics of deforming heterogeneous volcanic rocks and to provide a predictive tool. Zhu et al. (2010) provide an analytical approximation for the pore-emanating crack model such that the uniaxial compressive

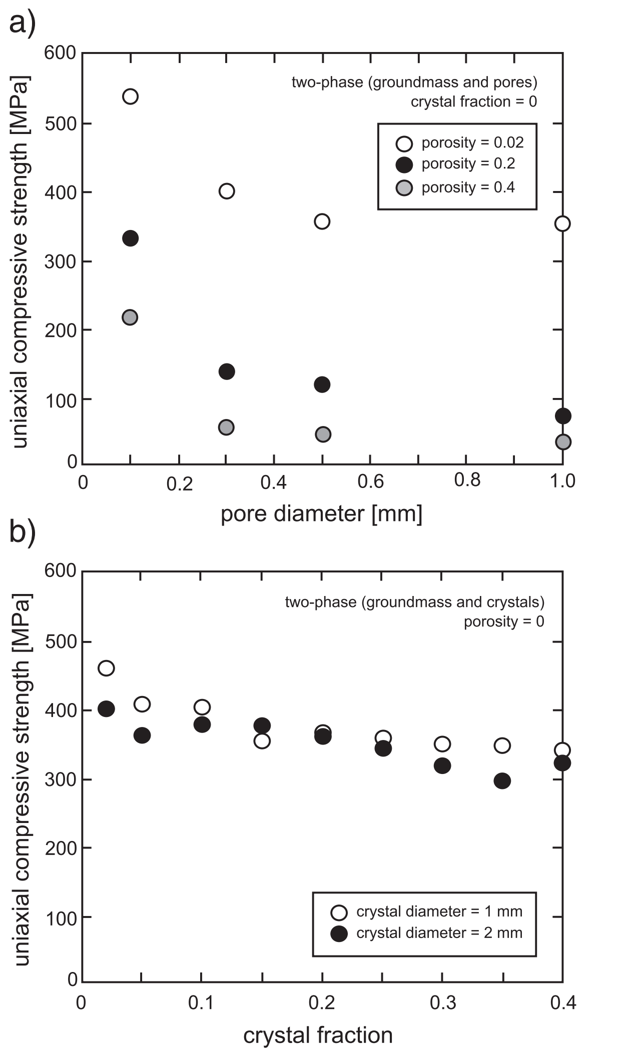

Fig. 6. The influence of heterogeneity diameter (pores and crystals) on the strength of two-phase volcanic rocks. (a) A plot of uniaxial compressive strength as a function of pore diameter for two-phase (groundmass and pores) simulations (simulation output from Heap et al., 2014b). White circles — simulations containing a porosity of 0.02; black circles — 0.2 porosity; grey circles — 0.4 porosity. (b) A plot of uniaxial compressive strength as a function of crystal fraction for two-phase (groundmass and crystals) simulations. White circles — simulations with a crystal diameter of 1 mm; black circles — crystal diameter of 2 mm.

strength UCS of porous rocks is a function of porosity ϕ_p, the fracture toughness K_{IC}, and the pore radius r:

$$UCS = \frac{a \cdot K_{IC}}{\phi_p{}^b \sqrt{\pi r}}. \quad (2)$$

For a constant K_{IC}, Zhu et al. (2010) find that the constants a and b are 1.325 and 0.414, respectively. These coefficient approximations are found for the 2D solution from Sammis and Ashby (1986) and so are directly applicable to our 2D simulations. This model has been used to describe the strength of various porous materials, including sandstones (e.g., Baud et al., 2014), limestones (e.g., Zhu et al., 2010), and volcanic materials (e.g., Zhu et al., 2011; Vasseur et al., 2013; Heap et al., 2014a, 2015c). We apply this same model to our simulated model results by calibrating the constants a and b against the crystal-free simulations presented in Heap et al. (2014b). Using the K_{IC} for defect-free borosilicate glass for the groundmass of 0.7 MPa m$^{0.5}$ (Wiederhorn, 1969), this calibration yields $a = 1.5$ and $b = 0.7$ for our system. Our choice of K_{IC} is validated by the agreement between our simulated

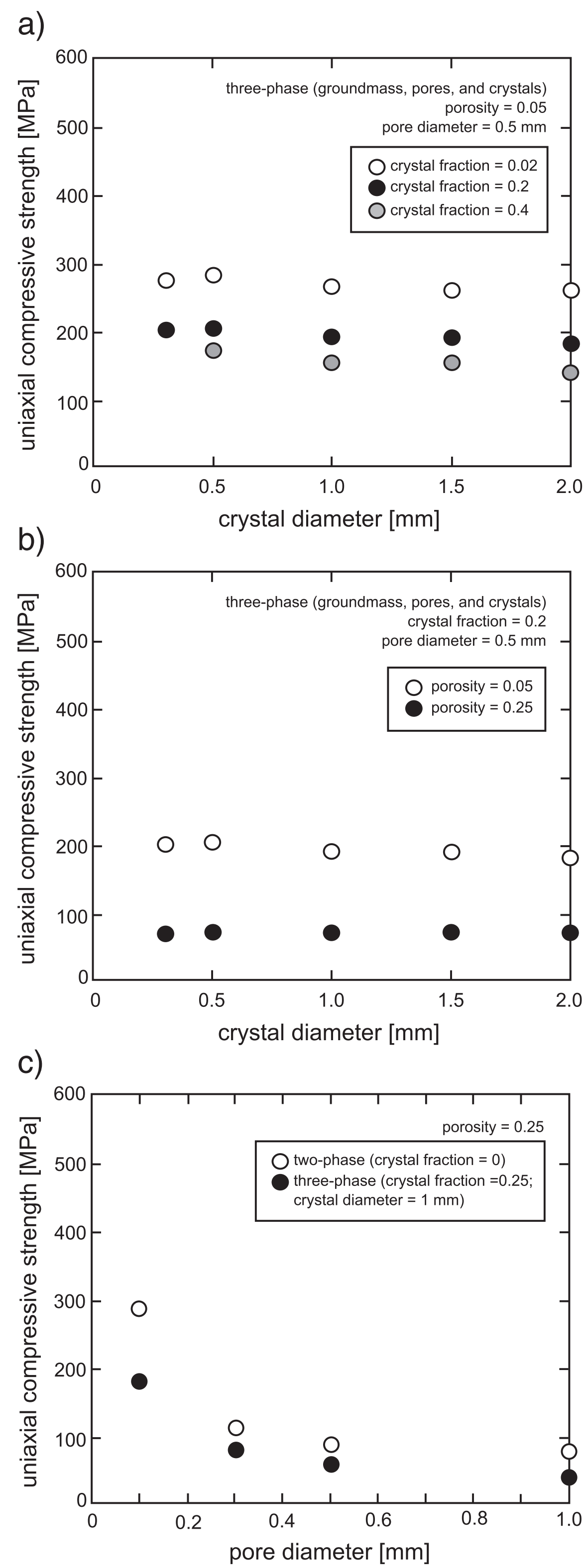

Fig. 7. The influence of heterogeneity diameter (pores and crystals) on the strength of three-phase volcanic rocks. (a) A plot of uniaxial compressive strength as a function of crystal diameter for three-phase simulations. White circles — simulations containing a crystal fraction of 0.02; black circles — 0.2 crystal fraction; grey circles — 0.4 crystal fraction. (b) A plot of uniaxial compressive strength as a function of crystal diameter for three-phase simulations. White circles — simulations containing a porosity of 0.05; black circles — 0.25 porosity. (c) A plot of uniaxial compressive strength as a function of pore diameter for two- (white circles) and three-phase (black circles) simulations.

strength at zero porosity (553 MPa) and the strength of porosity-free borosilicate glass reported in Vasseur et al. (2013) (~ 600 MPa). The analytical form of the Sammis and Ashby (1986) model (Eq. (2)) does not consider the influence of crystals on the compressive strength, a variable that, according to our modelling approach, will lower strength (Fig. 2b). Here therefore we recast the model to use ϕ_p' in place of ϕ_p, thus rescaling the volumes such that the pores occupy the effective medium and are enriched or crowded by the increasing crystal fraction. This yields a sample specific form of the pore-emanating crack model for the strength of heterogeneous volcanic materials:

$$UCS = \frac{1.5 \cdot K_{IC}}{\phi_p'^{\,0.7}\sqrt{\pi r}}. \qquad (3)$$

We find that the solution to this model (Eq. (3)), using K_{IC} = 0.7 MPa m$^{0.5}$, captures well the strength of our two- and three-phase simulations over a range of crystal and pore fractions relevant to volcanic systems (Fig. 8a). We highlight that, by implementing an effective medium approach, we treat the sample groundmass as a continuum that is weakened by the addition of porosity and, strictly speaking, K_{IC} should decrease with increasing porosity. Therefore, although direct comparison with micromechanical models such as the pore-emanating crack model should be considered with caution, we emphasise here that our approach works well (Fig. 8). The loss of fidelity in our selection of a constant K_{IC} explains the discrepancy between the simulations and Eq. (3) at low ϕ_p'.

To test the predictive power of our model, we can compare our modelled curves with data from experimental studies on the uniaxial compressive strength of volcanic materials for which the crystal content and porosities are known (Fig. 8b and c). We use data for variably-porous block-and-ash flow deposits (dacite) from Mt. Meager volcano, Canada (Heap et al., 2015c), andesitic lavas from Volcán de Colima, Mexico (Heap et al., 2014a) and Mount Shasta, USA (Smith et al., 2009), basalt from Iceland (Heap et al., 2010), and variably sintered borosilicate glass particles (Vasseur et al., 2013, 2015). We highlight that the samples used in these studies have very similar, or identical, dimensions (diameter and length) to that of the numerical samples presented in this study (sample dimensions for the above-mentioned studies are available in the figure caption of Fig. 8). These materials have a wide range of porosities and we take a mean crystal volume fraction of 0.25, 0.5, 0.17, 0, and 0, respectively (Smith et al., 2009; Heap et al., 2010, 2014a, 2015c; Vasseur et al., 2013, 2015). However, although we know their porosities and crystal contents, the remaining parameters in the model (Eq. (3)) are less well constrained. Both Fig. 8b and c show graphs of uniaxial compressive strength against effective porosity for the mined experimental data. Fig. 8b contains modelled strength curves for different values of K_{IC} for a constant pore diameter (0.5 mm) and Fig. 8c contains modelled strength curves for different pore diameters of a constant K_{IC} (0.7 MPa m$^{0.5}$). While we find that the data plot along similar trajectories as our modelled curves (Fig. 8b and c), it is clear that there are differences. When assessing datasets from 3D heterogeneous samples, critical shortcomings of the widely-used Eq. (2) are (1) it is a 2D approximation, (2) K_{IC} is presumed to be independent of the microstructural elements, and (3) the pore diameters are difficult to constrain.

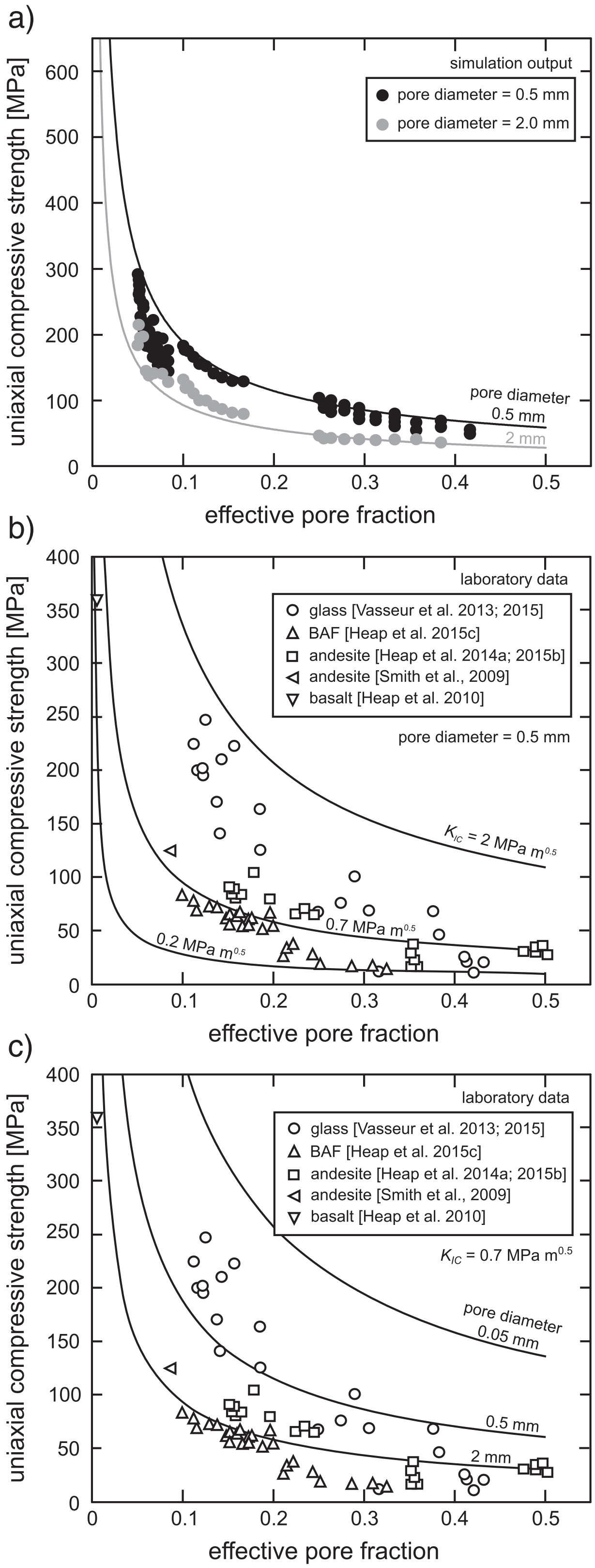

Fig. 8. Uniaxial compressive strength as a function of effective pore fraction. (a) Uniaxial compressive strength as a function of effective pore fraction for the simulated output for a pore diameter of 0.5 mm (black circles) and 2 mm (grey circles). Modelled curves are calculated using Eq. (2) using a pore diameter of 0.5 mm (black curve) and 2 mm (grey curve). Panels (b) and (c) show the same graph of uniaxial compressive strength as a function of effective pore fraction for a selection of mined experimental data: borosilicate glass (Vasseur et al., 2013, 2015; white circles; sample size: 25 mm in diameter and 50 mm in length), welded block-and-ash flow deposits (BAF; Heap et al., 2015b; white triangles; sample size: 20 mm in diameter and 40 mm in length), andesite lava from Volcán de Colima (Heap et al. 2014b, 2015a; sample size: 20 mm in diameter and 40 mm in length), basalt from Iceland (Heap et al., 2010; sample size: 25 mm in diameter and 75 mm in length), and andesite from Mt. Shasta (USA; Smith et al., 2009; sample size: 25 mm in diameter and 75 mm in length). Panel (b) contains modelled curves (Eq. (2)) for different values of K_{IC} for a constant pore diameter (pore diameter = 0.5 mm). Panel (c) contains modelled curves (Eq. (3)) for different pore diameters for a constant value of K_{IC} (K_{IC} = 0.7 MPa m$^{0.5}$).

On the microscale, fractures in natural rocks must invariably propagate through either the groundmass or crystal. Therefore, perhaps the most appropriate value of K_{IC} is that of the glass (K_{IC} = 0.7 MPa m$^{0.5}$, Wiederhorn, 1969) or the crystal. Unfortunately, while the K_{IC} of common rock-forming minerals such as quartz and calcite are well established, corresponding data for minerals typical of volcanic rocks are extremely sparse (Atkinson and Meredith, 1987). Further complication arises when one considers that microcracks often grow along weak clast interfaces (Zhu et al., 2011; Heap et al., 2015c) resulting in a K_{IC} lower than that of for the mineral constituents of the rock (see Tromans and Meech, 2002). We anticipate that particle/crystal boundary microcrack growth will be more prevalent in poorly-consolidated deposits, such as tuffs and welded deposits (Zhu et al., 2011; Heap et al., 2015c), and highly-crystallised materials. For example, Heap et al. (2015b) found that a K_{IC} of 0.15 MPa m$^{0.5}$ well describes the strength of the variably-porous block-and-ash flow deposits from Mt. Meager, citing that microcracks likely propagated along the boundaries of particles, rather than travelling through them. Indeed, a K_{IC} of 0.15 MPa m$^{0.5}$ is much lower than that of glass (K_{IC} = 0.7 MPa m$^{0.5}$, Wiederhorn, 1969) or feldspar (K_{IC} = 0.3–0.4 MPa m$^{0.5}$ for microcline, Atkinson and Avdis, 1980). Therefore, the values of K_{IC} measured for volcanic rocks, which can be as high as 2.5 MPa m$^{0.5}$ (e.g., Meredith and Atkinson, 1983; Atkinson and Meredith, 1987; Balme et al., 2004; Smith et al., 2009; Nara et al., 2012), are perhaps not suitable for the micromechanical model presented here. This notion is supported by the fact that, for a constant pore diameter of 0.5 mm, a value of K_{IC} of 2 MPa m$^{0.5}$ grossly overestimates rock strength (Fig. 8b). The choice of K_{IC} used in the model (Eq. (2)) should be considered on a case-by-case basis. While the K_{IC} for low-porosity or glassy rocks may be well approximated using a value close to that of the glass (K_{IC} = 0.7 MPa m$^{0.5}$, Wiederhorn, 1969), we highlight that highly-crystallised, poorly-consolidated/welded (e.g., Zhu et al., 2011; Heap et al., 2015c), and intensely hydrothermally altered (e.g., Pola et al., 2012, 2014; Wyering et al., 2014, 2015) rocks may be best represented by a much lower value (K_{IC} = 0.1–0.3 MPa m$^{0.5}$).

As outlined above, volcanic rocks can contain a wide pore size distribution (e.g., Wright et al., 2009; Shea et al., 2010; Heap et al., 2014a). However, the model (Eq. (3)) assumes that the pore radius is constant. A fundamental question thus arises: which pore radius should be used in the model? If we assume K_{IC} = 0.7 MPa m$^{0.5}$ for the andesites from Volcán de Colima (crystal fraction = 0.5) then the most representative pore diameter (i.e., the pore size exerting the greatest influence on the strength) is between about 1 and 2.5 mm (Fig. 8c). This pore diameter corresponds closely to the maximum pore diameter measured in these rocks, which is typically 1 or 2 mm (Heap et al., 2014a). The idea that the maximum pore diameter dictates the strength of the rock was also discussed in Zhu et al. (2010). Based on this logic we suggest that, if a single pore radius should be used as the input parameter in our model (Eq. (3)), then the maximum is a good candidate to provide reasonable predictions of strength. However, a law for the continuously evolving pore diameter during vesiculation (e.g., Gonnermann and Manga, 2007) or during densification (e.g., Wadsworth et al., 2016), which couple ϕ and r as a function of time-dependent magma dynamics (preserved as edifice rocks on quench), would be valuable inputs to Eq. (2).

We conclude that our modelling approach can be used with predictive power when the crystal content, porosity, and maximum pore size are known; parameters that are routinely measured for rocks found at many active volcanoes.

6. Implications for volcanic systems

As magmas ascend to the Earth's surface they degas and crystallise, producing volcanic rocks with crystal and pore fractions that can vary from almost 0 to almost 1 (e.g. Brophy, 1991; Marsh, 1981; Blundy et al., 2006; Kueppers et al., 2005; Farquharson et al., 2015). In general, the degree to which such precipitated phases of heterogeneity form and grow is a function of undercooling and thus the supersaturation of elements in the melt phase. For example, if volatiles are significantly oversaturated in a particular aliquot of melt, a bubble will form (e.g., Gardner and Ketcham, 2011; Pichavant et al., 2013). In detail, the formation of bubbles or crystals is a strong function of the decompression rate and the temperature and pressure dependence of solubility of the volatile element(s) (Toramaru, 2006; Hamada et al., 2010). After nucleation, the growth of heterogeneity phases is mostly limited by the mass diffusivity of the supersaturated element(s) (e.g., Gonnermann and Manga, 2007). These constraints on how heterogeneity is formed from an imagined homogeneous melt at depth directly inform work that compares the phases formed in pressure- and temperature-varied experiments with those in erupted rocks to constrain the ascent rate and temperature of conduit magma leading to eruption (e.g., Martel and Schmidt, 2003; Martel, 2012; Castro and Dingwell, 2009). In concert, the dependence of heterogeneity on the ascent path and composition of the magma suggests a tantalizing link between this pathway and the strength of the erupted rock. Recent work, for example, has shown that heterogeneity and strength is a key parameter in controlling the effectiveness of failure forecasting (Vasseur et al., 2015). Here we explore two case examples of volcanic eruptions that resulted in deposits containing high or low degrees of heterogeneity: the 2008 eruption at Chaitén volcano (Chile) and historic eruptions from Volcán de Colima (Mexico).

The eruption of Chaitén volcano in May 2008 produced a large range of eruptive products, but included a near-aphyric obsidian containing, typically, a low porosity that now forms the base of the exposed dome (Castro et al., 2014). This erupted material, along with other obsidian-forming eruptions, is an interesting example of material that can reach the Earth's surface and preserve relative homogeneity. Castro and Dingwell (2009) showed that in this case the ascent rates were sufficiently high to bypass crystallisation. Our results suggest that at these obsidian-forming sites, the homogeneity can result in exceptionally strong deposits (falling on the far-left side of Fig. 8). The outgassing mechanism for obsidian-forming eruptions is not well constrained (Owen et al., 2013), and it has been proposed that fracturing followed by thorough sintering to dense melt is the mechanism (Castro et al., 2014). This mechanism would result in short lengthscale heterogeneity, such as spatial heterogeneity of remnant dissolved water concentration in the groundmass glass, akin to a shift in our homogeneity index m. Therefore, prior to sintering, the material strength would be lower and it is only by thorough viscous sintering that the heterogeneity (porosity in this case) is removed and the material strength increases (e.g., Heap et al., 2015c). Data from sintering experiments that propose to recreate this process using synthetic glass particles (Vasseur et al., 2013) and natural volcanic particles (Heap et al., 2014c, 2015c) are highly consistent with our effective medium approach (Fig. 8). We note that the same Chaitén eruption was accompanied by a Plinian explosive pumice-forming eruption with porosities of 0.2–0.8 (Castro et al., 2012; Alfano et al., 2012), which by contrast would be a highly heterogeneous and therefore weak deposit. A characteristic feature of rhyolitic eruptions is that periodic explosions that expel more heterogeneous materials accompany the effusive of lava (e.g., Schipper et al., 2013). We suggest that such activity would result in a bimodality of strength of the final volcanic materials.

By contrast, the Volcán de Colima volcanic edifice is composed of blocks of volcanic rock with a wide range of porosity, from 0.02 to 0.73 (Lavallée et al., 2012; Heap et al., 2014a; Farquharson et al., 2015; Lavallée et al., 2016), and a high crystal fraction, typically about 0.5 (Lavallée et al., 2007; Heap et al., 2014a, 2015b). In other words, the rocks are very heterogeneous and, for the most part, fall on the right side of Fig. 8. In terms of heterogeneity, these materials are typical of the rocks forming andesitic arc volcanoes, such as Merapi (Indonesia) or Mt. Ruapehu (New Zealand), which typically host a wide range of porosity (e.g., Mueller et al., 2005). The highly heterogeneous nature of the rocks forming andesitic arc volcanoes makes them weak, a weakness perhaps exemplified by their frequently-collapsing nature: there have been at least five major collapses at Volcán de Colima in the last 18,500 years (e.g., Stoopes and Sheridan, 1992; Cortés et al., 2010).

7. Concluding remarks and perspectives

Our modelling highlights that heterogeneities (pores and crystals) serve to decrease the strength of volcanic rocks. In detail, increasing porosity commands a greater strength reduction than increasing the crystal fraction. Further, strength at a constant porosity is reduced by increasing the pore diameter, but strength at a constant crystal fraction is unaffected by increasing the crystal diameter. To account for the weakening influence of pores and crystals as a single variable — the "heterogeneity" — we use an effective medium approach in which we define sample heterogeneity using an effective pore fraction. When the strength of more than 200 simulated samples is plotted as a function of their effective porosity, we find that, for a given pore diameter, the model output falls on a single curve. A modified version of Sammis and Ashby's (1986) pore-emanating crack model for 2D porous media, recast to include the effective porosity rather than the porosity and calibrated for our crystal-free simulations, is in good agreement with published experimental data for which the porosity and crystal content are known (although we highlight some difficulties in constraining two of the input parameters, namely the representative pore radius and the fracture toughness, and in the 2D to 3D discrepancy). We therefore present herein an analytical tool that can be used to estimate the strength of volcanic rock when the porosity, crystal fraction, and maximum pore diameter are known.

Acknowledgements

The authors of this study acknowledge the support of two Partenariats Hubert Curien (PHC) grants: Xu Guangqi grant number 32195NC and Procope grant number 332065SG. Both grants were funded and implemented by the Ministry of Foreign Affairs (MAEDI) and the Ministry of Higher Education and Research (MENESR) in France, with help from the French Institute of the Chinese Embassy of France in China (for the Xu Guangqi grant) and the Deutscher Akademischer Austauschdienst (DAAD) in Germany (for the Procope grant). Tao Xu acknowledges the National Natural Science Foundation of China (grant number 51474051), the National Basic Research Programme of China (grant number 2013CB227900), and Fundamental Research Funds for the Central Universities of China (grant number N130501002). Funding for Fabian Wadsworth was provided by the European Union's Seventh Programme for research, technological development and demonstration under grant agreement No. 282759 (VUELCO). M. Heap acknowledges stimulating discussions with P. Baud. We acknowledge the constructive comments of two anonymous reviewers and the editor, Joan Martí.

References

Alfano, F., Bonadonna, C., Gurioli, L., 2012. Insights into eruption dynamics from textural analysis: the case of the May, 2008, Chaitén eruption. Bull. Volcanol. 74, 2095–2108.

Al-Harthi, A.A., Al-Amri, R.M., Shehata, W.M., 1999. The porosity and engineering properties of vesicular basalt in Saudi Arabia. Eng. Geol. 54, 313–320.

Applegarth, L.J., Tuffen, H., James, M.R., Pinkerton, H., Cashman, K.V., 2012. Direct observations of degassing-induced crystallization in basalts. Geology http://dx.doi.org/10.1130/G33641.1.

Atkinson, B.K., Avdis, V., 1980. Fracture mechanics parameters of some rock-forming minerals determined using an indentation technique. Int. J. Rock Mech. Min. Sci. Geomech. Abstr. 17, 383–386.

Atkinson, B.K., Meredith, P.G., 1987. Experimental fracture mechanics data for rocks and minerals. In: Atkinson, B.K. (Ed.), Fracture Mechanics of Rock. Academic Press, London.

Balme, M.R., Rocchi, V., Jones, C., Sammonds, P.R., Meredith, P.G., Boon, S.A., 2004. Fracture toughness measurements on igneous rocks using a high-pressure, high-temperature rock fracture mechanics cell. J. Volcanol. Geotherm. Res. 132, 159–172.

Baud, P., Wong, T.-f., Zhu, W., 2014. Effects of porosity and crack density on the compressive strength of rocks. Int. J. Rock Mech. Min. Sci. 67, 202–211.

Biggs, J., Mothes, P., Ruiz, M., Amelung, F., Dixon, T.H., Baker, S., Hong, S.-H., 2010. Stratovolcano growth by co-eruptive intrusion: the 2008 eruption of Tungurahua Ecuador. Geophys. Res. Lett. 37, 21. http://dx.doi.org/10.1029/2010GL044942.

Blundy, J., Cashman, K.V., Humphreys, M., 2006. Magma heating by decompression-driven crystallization beneath andesite volcanoes. Nature 443, 76–80.

Borgia, A., Linneman, S.R., 1990. On the mechanisms of lava flow emplacement and volcano growth: Arenal, Costa Rica, lava flows and domes. IAVCEI Proc. Volcanol. 2, 208–243.

Brophy, J.G., 1991. Composition gaps, critical crystallinity, and fractional crystallization in orogenic (calc-alkaline) magmatic systems. Contrib. Mineral. Petrol. 109, 173–182.

Caricchi, L., Burlini, L., Ulmer, P., Gerya, T., Vassalli, M., Papale, P., 2007. Non-Newtonian rheology of crystal-bearing magmas and implications for magma ascent dynamics. Earth Planet. Sci. Lett. 264, 402–419.

Cashman, K.V., Marsh, B.D., 1988. Crystal size distribution (CSD) in rocks and the kinetics and dynamics of crystallization II: Makaopuhi lava lake. Contrib. Mineral. Petrol. 99, 292–305.

Castro, J., Dingwell, D.B., 2009. Rapid ascent of rhyolitic magma at Chaitén volcano, Chile. Nature 461, 780–783.

Castro, J.M., Cordonnier, B., Tuffen, H., Tobin, M.J., Pusker, L., Martin, M.C., Bechtel, H.A., 2012. The role of melt-fracture degassing in defusing explosive rhyolite eruptions at volcán Chaitén. Earth Planet. Sci. Lett. 333-334, 63–69.

Castro, J., Bindeman, I.N., Tuffen, H., Schipper, C.I., 2014. Explosive origin of silicic lava: textural and δD–H_2O evidence for pyroclastic degassing during rhyolite effusion. Earth Planet. Sci. Lett. 405, 52–61.

Cordonnier, B., Hess, K.-U., Lavallée, Y., Dingwell, D.B., 2009. Rheological properties of dome lavas: case study of Unzen volcano. Earth Planet. Sci. Lett. 279, 263–272.

Cordonnier, B., Caricchi, L., Pistone, M., Castro, J., Hess, K.-U., Gottschaller, S., Manga, M., Dingwell, D.B., Burlini, L., 2012. The viscous–brittle transition of crystal-bearing silicic melt: direct observation of magma rupture and healing. Geology 40, 611–614.

Cortés, A., Garduño, V.H., Macías, J.L., Navarro-Ochoa, C., Komorowski, J.C., Saucedo, R., Gavilanes, J.C., 2010. Geologic mapping of the Colima volcanic complex (Mexico) and implications for hazard assessment. Geol. Soc. Am. Spec. Pap. 464, 249–264.

Farquharson, I.J., Heap, M.J., Varley, N., Baud, P., Reuschlé, T., 2015. Permeability and porosity relationships of edifice-forming andesites: a combined field and laboratory study. J. Volcanol. Geotherm. Res. 297, 52–68.

Gardner, J.E., Ketcham, R.A., 2011. Bubble nucleation in rhyolite and dacite melts: temperature dependence of surface tension. Contrib. Mineral. Petrol. 162, 929–943.

Gondé, C., Martel, C., Pichavant, M., Bureau, H., 2011. In situ bubble vesiculation in silicic magmas. Am. Mineral. 96, 111–124.

Gonnermann, H.M., Manga, M., 2007. The fluid mechanics inside a volcano. Annu. Rev. Fluid Mech. 39, 321–356.

Gonnermann, H.M., Manga, M., 2013. Dynamics of magma ascent in the volcanic conduit. In: Fagents, S.A., Gregg, T.K.P., Lopes, R.M.C. (Eds.), Modeling Volcanic Processes: The Physics and Mathematics of Volcanism. Cambridge University Press, Cambridge.

Gutmann, J.T., 1977. Textures and genesis of phenocrysts and megacrysts in basaltic lavas from the Pinacate volcanic field. Am. J. Sci. 277, 833–861.

Hamada, M., Laporte, D., Cluzel, N., Koga, K.T., Kawamoto, T., 2010. Simulating bubble number density of rhyolitic pumices from Plinian eruptions: constraints from fast decompression experiments. Bull. Volcanol. 72, 735–746.

Hammer, J.E., 2004. Crystal nucleation in hydrous rhyolite: experimental data applied to classical theory. Am. Mineral. 89, 1673–1679.

Heap, M.J., Faulkner, D.R., Meredith, P.G., Vinciguerra, S., 2010. Elastic moduli evolution and accompanying stress changes with increasing crack damage: implications for stress changes around fault zones and volcanoes during deformation. Geophys. J. Int. 183, 225–236.

Heap, M.J., Lavallée, Y., Laumann, A., Hess, K.-U., Meredith, P.G., Dingwell, D.B., 2012. How tough is tuff in the event of fire? Geology 40, 311–314.

Heap, M.J., Lavallée, Y., Petrakova, L., Baud, P., Reuschlé, T., Varley, N., Dingwell, D.B., 2014a. Microstructural controls on the physical and mechanical properties of edifice-forming andesites at Volcán de Colima, Mexico. J. Geophys. Res. 119, 2925–2963.

Heap, M.J., Xu, T., Chen, C.-f., 2014b. The influence of porosity and vesicle size on the brittle strength of volcanic rocks and magmas. Bull. Volcanol. 76, 856. http://dx.doi.org/10.1007/s00445-014-0856-0.

Heap, M.J., Kolzenburg, S., Russell, J.K., Campbell, M.E., Welles, J., Farquharson, J.I., Ryan, A., 2014c. Conditions and timescales for welding block-and-ash flow deposits. J. Volcanol. Geotherm. Res. 289, 202–209.

Heap, M.J., Xu, T., Kushnir, A.R.L., Kennedy, B., Chen, C.-f., 2015a. Fracture of magma containing overpressurised pores. J. Volcanol. Geotherm. Res. 301, 180–190.

Heap, M.J., Farquharson, I.J., Baud, P., Lavallée, Y., Reuschlé, T., 2015b. Fracture and compaction of andesite in a volcanic edifice. Bull. Volcanol. 77, 55. http://dx.doi.org/10.1007/s00445-015-0938-7.

Heap, M.J., Farquharson, I.J., Wadsworth, F.B., Kolzenburg, S., Russell, J.K., 2015c. Timescales for permeability reduction and strength recovery in densifying magma. Earth Planet. Sci. Lett. 429, 223–233.

Hess, K.-U., Dingwell, D.B., 1996. Viscosities of hydrous leucogranitic melts: a non-Arrhenian model. Am. Mineral. 81, 1297–1300.

Jaeger, J., Cook, N.G.W., Zimmerman, R., 2007. Fundamentals in Rock Mechanics. fourth ed. Blackwell Publishing, London.

Jaupart, C., 1998. Gas loss from magmas through conduit walls during eruption. Geol. Soc. Lond., Spec. Publ. 145, 73–90.

Kaneko, K., 2002. Exogenous and endogenous growth of the Unzen lava dome examined by satellite infrared image analysis. J. Volcanol. Geotherm. Res. 116, 151–160.

Kendrick, J.E., Lavallée, Y., Hess, K.-U., Heap, M.J., Gaunt, H.E., Meredith, P.G., Dingwell, D.B., 2013. Tracking the permeable porous network during strain-dependent magmatic flow. J. Volcanol. Geotherm. Res. 260, 117–126.

Kueppers, U., Scheu, B., Spieler, O., Dingwell, D.B., 2005. Field-based density measurements as tool to identify preeruption dome structure: set-up and first results from Unzen volcano, Japan. J. Volcanol. Geotherm. Res. 141, 65–75.
Lavallée, Y., Hess, K.-U., Cordonnier, B., Dingwell, D.B., 2007. A non-Newtonian rheological flow law for highly-crystalline dome lavas. Geology 35, 843–846.
Lavallée, Y., Meredith, P.G., Dingwell, D.B., Hess, K.-U., Wassermann, J., Cordonnier, B., Gerik, A., Kruhl, J.H., 2008. Seismogenic lavas and explosive eruption forecasting. Nature 453, 507–510.
Lavallée, Y., Varley, N., Alatorre-Ibargüengoitia, M.A., Hess, K.-U., Kueppers, U., Mueller, S., Richard, D., Scheu, B., Spieler, O., Dingwell, D.B., 2012. Magmatic architecture of dome-building eruptions at Volcán de Colima, Mexico. Bull. Volcanol. 74, 249–260.
Lavallée, Y., Heap, M.J., Kueppers, U., Kendrick, J.E., Dingwell, D.B., 2016. The fragility of Volcán de Colima — a material constraint. In: Varley, N., Komorowski, J.C. (Eds.), Volcán de Colima: Managing the Threat. Springer-Verlag, Berlin Heidelberg.
Lemaitre, J., Chaboche, J.-L., 1990. Mechanics of Solid Materials. Cambridge University Press, Cambridge.
Mader, H.M., Llewellin, E.W., Mueller, S.P., 2013. The rheology of two-phase magmas: a review and analysis. J. Volcanol. Geotherm. Res. 257, 135–158.
Mangan, M., Cashman, K.V.N.S., 1993. Vesiculation of basaltic magma during eruption. Geology 21, 157–160.
Marsh, B.D., 1981. On the crystallinity, probability of occurrence, and rheology of lava and magma. Contrib. Mineral. Petrol. 78, 85–98.
Marsh, B.D., 1988. Crystal size distribution (CSD) in rocks and the kinetics and dynamics of crystallization. Contrib. Mineral. Petrol. 99, 277–297.
Martel, C., 2012. Eruption dynamics inferred from microlite crystallization experiments: application to plinian and dome-forming eruptions of Mt. Pelée (Martinique, Lesser Antilles). J. Petrol. 53, 699–725.
Martel, C., Schmidt, B.C., 2003. Decompression experiments as an insight into ascent rates of silicic magmas. Contrib. Mineral. Petrol. 144, 397–415.
Meredith, P.G., Atkinson, B.K., 1983. Stress corrosion and acoustic emission during tensile crack propagation in Whin Sill dolerite and other basic rocks. Geophys. J. Int. 75, 1–21.
Mueller, S., Melnik, O., Spieler, O., Scheu, B., Dingwell, D.B., 2005. Permeability and degassing of dome lavas undergoing rapid decompression: an experimental study. Bull. Volcanol. 67, 526–538.
Nara, Y., Morimoto, K., Hiroyoshi, N., Yoneda, T., Kaneko, K., Benson, P.M., 2012. Influence of relative humidity on fracture toughness of rock: implications for subcritical crack growth. Int. J. Solids Struct. 49, 2471–2481.
Navon, O., Lyakhovsky, V., 1998. Vesiculation processes in silicic magmas. Geol. Soc. Lond., Spec. Publ. 145, 27–50.
Odbert, H.M., Taisne, B., Gottsmann, J., 2015. Deposit loading and its effect on co-eruptive volcano deformation. Earth Planet. Sci. Lett. 413, 186–196.
Owen, J., Tuffen, H., McGarvie, D.W., 2013. Explosive subglacial rhyolitic eruptions in Iceland are fuelled by high magmatic H_2O and closed-system degassing. Geology 41, 251–254.
Pichavant, M., Di Carlo, I., Rotolo, S.G., Scaillet, B., Burgisser, A., Le Gall, N., Martel, C., 2013. Generation of CO_2-rich melts during basalt magma ascent and degassing. Contrib. Mineral. Petrol. 166, 545–561.
Pola, A., Crosta, G.B., Fusi, N., Barberini, V., Norini, G., 2012. Influence of alteration on physical properties of volcanic rocks. Tectonophysics 566-567, 67–86.
Pola, A., Crosta, G.B., Fusi, N., Castellanza, R., 2014. General characterization of the mechanical behaviour of different volcanic rocks with respect to alteration. Eng. Geol. 169, 1–13.
Sammis, C.G., Ashby, M.F., 1986. The failure of brittle porous solids under compressive stress states. Acta Metall. 34, 511–526. http://dx.doi.org/10.1016/0001-6160(86)90087-8.
Schaeffer, L.N., Kendrick, J.E., Oommen, T., Lavallée, Y., Chigna, G., 2015. Geomechanical rock properties of a basaltic volcano. Front. Earth Sci. 3, 29. http://dx.doi.org/10.3389/feart.2015.00029.
Schipper, C.I., Castro, J.M., Tuffen, H., James, M.R., How, P., 2013. Shallow vent architecture during hybrid explosive–effusive activity at Cordón Caulle (Chile, 2011–12): evidence from direct observations and pyroclast textures. J. Volcanol. Geotherm. Res. 262, 25–37.
Self, S., Thordarson, T., Keszthelyi, L., 1997. Emplacement of continental flood basalt lava flows. In: Mahoney, J.J., Coffin, M. (Eds.), Large Igneous Processes: Continental, Oceanic, and Planetary Flood Volcanism. American Geophysical Union, Washington.
Shea, T., Houghton, B.F., Gurioli, L., Cashman, K.V., Hammer, J.E., Hobden, B.J., 2010. Textural studies of vesicles in volcanic rocks: an integrated methodology. J. Volcanol. Geotherm. Res. 190, 271–289.
Smith, R., Sammonds, P.R., Kilburn, C.R.J., 2009. Fracturing of volcanic systems: experimental insights into pre-eruptive conditions. Earth Planet. Sci. Lett. 280 (221-219).
Sparks, R.S.J., 1978. The dynamics of bubble formation and growth in magmas: a review and analysis. J. Volcanol. Geotherm. Res. 3, 1–37.
Spohn, T., Hort, M., Fischer, H., 1988. Numerical simulation of the crystallization of multicomponent melts in thin dikes or sills: 1. The liquidus phase. J. Geophys. Res. 93, 4880–4894.
Stoopes, G.R., Sheridan, M.F., 1992. Giant debris avalanches from the Colima Volcanic Complex, Mexico: implications for long-runout landslides (>100 km) and hazard assessment. Geology 20, 299–302.
Tang, C.A., 1997. Numerical simulation of progressive rock failure and associated seismicity. Int. J. Rock Mech. Min. Sci. 34, 249–261.
Toramaru, A., 1989. Vesiculation process and bubble size distributions in ascending magmas with constant velocities. J. Geophys. Res. 94 (B12), 17523–17542.
Toramaru, A., 2006. BND (bubble number density) decompression rate meter for explosive volcanic eruptions. J. Volcanol. Geotherm. Res. 154, 303–316.
Tromans, D., Meech, J.A., 2002. Fracture toughness and surface energies of minerals: theoretical estimates for oxides, sulphides, silicates and halides. Miner. Eng. 15, 1027–1041.
Truby, J.M., Mueller, S.P., Llewellin, E.W., Mader, H.M., 2015. The rheology of three-phase suspensions at low bubble capillary number. Proc. R. Soc. London, Ser. A 471. http://dx.doi.org/10.1098/rspa.2014.0557.
Vasseur, J., Wadsworth, F.B., Lavallée, Y., Hess, K.-U., Dingwell, D.B., 2013. Volcanic sintering: timescales of viscous densification and strength recovery. Geophys. Res. Lett. 40, 5658–5664.
Vasseur, J., Wadsworth, F.B., Lavallée, Y., Bell, A.F., Main, I.G., Dingwell, D.B., 2015. Heterogeneity: the key to failure forecasting. Sci. Rep. 5. http://dx.doi.org/10.1038/srep13259.
Voight, B., 2000. Structural Stability of Andesite Volcanoes and Lava Domes. Causes and Consequences of Eruptions of Andesite Volcanoes (May 15, 2000). Philosophical Transactions: *Mathematical, Physical and Engineering Sciences* 358, No. 1770, pp. 1663–1703.
Voight, B., Elsworth, D., 1997. Failure of volcanic slopes. Géotechnique 47, 1–31.
Wadsworth, F.B., Vasseur, J., von Aulock, F.W., Scheu, B., Lavallée, Y., Hess, K.-U., Dingwell, D.B., 2014. Nonisothermal viscous sintering of volcanic ash. J. Geophys. Res. 119, 8792–8804. http://dx.doi.org/10.1002/2014JB011453.
Wadsworth, F.B., Vasseur, J., Scheu, B., Kendrick, J.E., Lavallée, Y., Dingwell, D.B., 2016. Universal scaling for fluid permeability during volcanic welding and sediment diagenesis. Geology http://dx.doi.org/10.1130/G37559.1.
Weibull, W., 1951. A statistical distribution function of wide applicability. J. Appl. Mech. 18, 293–297.
Wiederhorn, S.M., 1969. Fracture surface energy of glass. J. Am. Ceram. Soc. 52 (2), 99–105.
Wong, T.-f., Wong, R.H.C., Chau, K.T., Tang, C.A., 2006. Microcrack statistics, Weibull distribution and micromechanical modeling of compressive failure in rock. Mech. Mater. 38, 664–681.
Wright, H.M.N., Cashman, K.V., Gottesfeld, E.H., Roberts, J.J., 2009. Pore structure of volcanic clasts: measurements of permeability and electrical conductivity. Earth Planet. Sci. Lett. 280, 93–104.
Wyering, L.D., Villeneuve, M.C., Wallis, I.C., Siratovich, P.A., Kennedy, B.M., Gravely, D.M., Cant, J.L., 2014. Mechanical and physical properties of hydrothermally altered rocks, Taupo Volcanic Zone, New Zealand. J. Volcanol. Geotherm. Res. 288, 76–93.
Wyering, L.D., Villeneuve, M.C., Wallis, I.C., Siratovich, P.A., Kennedy, B.M., Gravely, D.M., 2015. The development and application of the alteration strength index equation. Eng. Geol. 199, 48–61.
Xu, T., Tang, C.-A., Zhao, J., Li, L., Heap, M.J., 2012. Modelling the time-dependent rheological behaviour of heterogeneous brittle rocks. Geophys. J. Int. 189, 1781–1796.
Zhu, W., Baud, P., Wong, T.-F., 2010. Micromechanics of cataclastic pore collapse in limestone. J. Geophys. Res. 115 (B4). http://dx.doi.org/10.1029/2009JB006610.
Zhu, W., Baud, P., Vinciguerra, S., Wong, T.-F., 2011. Micromechanics of brittle faulting and cataclastic flow in Alban Hills tuff. J. Geophys. Res. 116, B06209. http://dx.doi.org/10.1029/2010JB008046.